Using Power Watersheds to Segment Benign Thyroid Nodules in Ultrasound Image Data

Eva Kollorz[1,2], Elli Angelopoulou[1], Michael Beck[2], Daniela Schmidt[2], Torsten Kuwert[2]

[1] Pattern Recognition Lab, Friedrich-Alexander-University Erlangen-Nuremberg,
[2] Department of Nuclear Medicine, University Hospital Erlangen
Eva.Kollorz@informatik.uni-erlangen.de

Abstract. Thyroid nodule segmentation is a hard task due to different echo structures, textures and echogenicities in ultrasound (US) images as well as speckle noise. Currently, a typical clinical evaluation involves the manual, approximate measurement in two section planes in order to obtain an estimate of the nodule's size. The aforementioned nodule attributes are recorded on paper. We propose instead the semi-automatic segmentation of 2D slices of acquired 3D US volumes with power watersheds (PW) independent of the nodule type. We tested different input seeds to evaluate the potential of the applied algorithm. On average we achieved a 76.81% sensitivity, 88.95% precision and 0.81 Dice coefficient. The runtime on a standard PC is about 0.02 seconds which indicates that the extension to 3D volume data should be feasible.

1 Introduction

A study of human thyroid glands throughout Germany in 2001/2002 showed that every fourth citizen has nodules in his thyroid gland. Thus, modern screening methods are necessary for controlling the progress of nodule growth. Among several diagnostic modalities, US imaging is the most popular one, partly due to its low cost, ease of use and lack of radiation. There are different techniques for studying thyroid nodules: US elastography, contrast-enhanced US (CEUS) [1],

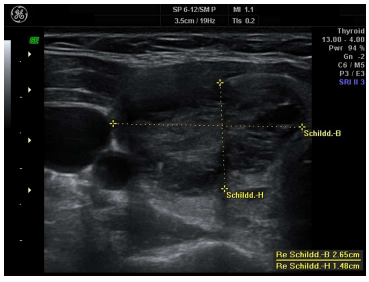

Fig. 1. Screen shot of the 2D measurement (axial section plane) of an echo complex thyroid nodule, partial input for the ellipsoid formula; compare to Fig. 3: last row (sagittal section plane).

color power Doppler US [1] and "traditional" 2D/3D US with/without guided fine-needle aspiration biopsy [2]. During a typical US examination of the thyroid gland, a physician manually measures the volume of a nodule with the ellipsoid formula (see Fig. 1). He also records the echo structure (solid, mixed or cystic), texture (homogeneous, heterogeneous) and echogenicity (iso-, hyper- or hypoechoic) in the patient's chart. Additionally, 2D print-outs of the two section planes are added to the chart. This procedure becomes complex if there are multiple nodules of different types. The findings of the examination can also vary with the physician's experience. The longterm goal of this project is to develop a computerized system which (semi-)automatically detects, accurately measures and classifies the different nodule types in the thyroid gland (see Fig. 3, middle column).

Medical studies have correlated the appearance of nodules with their benignity and malignancy [2,3]. These studies were based on visual inspection of size, calcifications, blurred margins and echogenicity. Recently there has been interest in automating the nodule identification process [4,5]. However, because of the big variation in nodule appearance, existing methods make restrictive assumptions. For example, Maroulis *et al.* [4] study only hypoechoic thyroid nodules. Tsantis *et al.* [5] use a multi-scale structure model in combination with an explicit circular shape prior, which may fail in axial section planes due to a possible confusion with circular arteries and veins. Furthermore, they work mainly with iso- and hypoechoic nodules.

Instead of explicitly incorporating such restrictive assumptions in our system, we allow the user to provide additional information in an easy-to-use intuitive interface. We work with 3D US volumes of benign nodules and try to segment them reliably in order to capture changes in echo structure, texture and echogenicity. Working with 3D US has the advantage of utilizing the entire volume, e.g. for echogenicity and echo texture analysis and for precise volume estimation (if there is not an ellipsoidal shape). Though our ultimate goal is to classify the different nodule types, this is currently not feasible due to the very limited amount of training image data. Therefore this paper focuses on a semi-automatic approach for segmenting the different benign nodule types.

2 Materials and Methods

As an initial baseline we tested the traditional watershed segmentation method. Please note that certain parameters like flood level, minimum intensity or number of regions have to be adjusted. Fig. 2 shows on the left side the gradient magnitude image, on the right side the result of the watershed segmentation. The nodule structure was not extracted satisfactorily. Since the appearance of nodules can vary significantly and is not sufficiently distinct from the surrounding structure, we believe that a semi-automatic segmentation approach is more appropriate.

Couprie *et al.* [6] proposed a new family of seeded segmentation algorithms called **power watersheds** (PW). They extended the watershed algorithm into

a general framework for seeded/semi-automatic image segmentation which contains graph cuts (GC), random walker (RW), and shortest path optimization algorithms. Each image pixel is associated with a graph node and nodes are connected with edges to their four neighboring pixels. Each edge has a weight that is determined by a similarity measure, e.g. intensity, of the pixels at the endpoints of the edge. A high weight indicates high similarity between the two pixel intensities. The watershed of a function (seen as a topological surface) is composed by the locations from which a drop of water could flow towards different minima. In a framework of edge-weighted graphs, the watershed is defined as a cut relative to the regional minima/maxima of the weight function. Couprie *et al.* [6] showed that GC and RW segmentations correspond to a maximum spanning forest (MSF) [7]. The MSF computation is a key factor in the computational efficiency. PW is based on Kruskal's algorithm for MSF computation and on RW for plateaus (edge sets with same weights connected to more than one labeled tree).

As part of our analysis we investigated different types of seeds: single points,

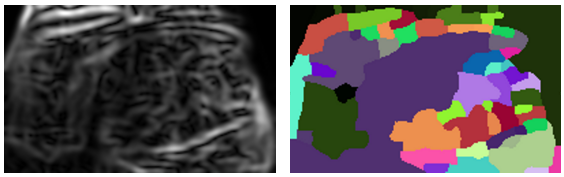

Fig. 2. Left: Gradient magnitude image of Example 6), right: Watershed segmentation result.

open and closed curves. Different benign nodule type categories were evaluated (see Fig. 3). The available image data contains only the region of interest (ROI), not the whole thyroid gland. The volumes were obtained from the General Electric Healthcare ultrasound system Voluson 730 Pro with a 3D RSP 6-16 MHz small part probe. The volume size varies between $199 \times 65 \times 181$ - $199 \times 153 \times 169$ with an isotropic voxel size of 0.28594 - 0.339378 mm. At this stage, we only use 2D slices for evaluating the algorithm.

3 Results

Fig. 3 shows the seed placement, the original US slice and the segmentation results of PW and the two gold standard segmentations (GSS). Note that for the GSS the 3D volume is more informative when traversing through the slices than by analyzing single 2D slice. Sensitivity (SE), precision (PRE) and Dice coefficient (DICE) are calculated for the seven examples. Additionally, in Table 1 the Jaccard index (JAC) of the two GSS as well as the JAC of the PW result and each GSS is given. The computation time is on average 0.02 seconds for one slice on a standard PC (Intel® Core ™2 Duo, 2.49 GHz, 3,5 GB of RAM).

Example	GSS 1 (green)				GSS 2 (red)				JAC
	SE [%]	PRE [%]	DICE	JAC	SE [%]	PRE [%]	DICE	JAC	GSS
1	74.79	85.09	0.80	0.66	57.37	95.98	0.72	0.56	0.68
2	94.96	90.38	0.93	0.86	94.38	92.43	0.93	0.87	0.88
3	91.70	67.26	0.78	0.63	93.91	72.19	0.81	0.68	0.87
4	76.25	90.39	0.83	0.70	72.34	90.11	0.80	0.67	0.93
5	70.00	97.34	0.81	0.68	71.79	98.60	0.83	0.71	0.88
6 i)	61.78	89.73	0.73	0.57	60.40	92.80	0.73	0.57	0.90
6 ii)	78.11	89.20	0.83	0.71	77.69	93.88	0.85	0.73	0.90

Table 1. Quantitative results of the six examples: sensitivity (SE), precision (PRE), Dice coefficient (DICE), Jaccard index (JAC) of two gold standard segmentations (GSS) compared to the PW result. JAC GSS shows the JAC of the two GSS.

4 Discussion

Some of our image data is problematic in terms of complex echogenicity patterns, e.g. echo complex nodule or hypoechoic nodules with cystic parts (see Fig. 3). Better results can be achieved with more user input (see Fig. 3: Example 6) but has to be study carefully. It can be seen that the different occurrences of the nodule types are segmented roughly (see Examples 4 and 6 ii). Example 1 shows a higher deviation for the two GSS than the other examples. An extension to 3D is planned as well as the classification of different nodule types after segmentation, e.g. in follow-up studies.

References

1. Bartolotta TV, Midiri M, Galia M, Runza G, Attard M, Savoia G, et al. Qualitative and quantitative evaluation of solitary thyroid nodules with contrast-enhanced ultrasound: initial results. Eur Radiol. 2006;16:2234–2241.
2. Iannuccilli JD, Cronan JJ, Monchik JM. Risk for Malignancy of Thyroid Nodules as Assessed by Sonographic Criteria. J Ultrasound Med. 2004;23:1455–1464.
3. Cappelli C, Castellano M, Pirola I, Cumetti D, Agosti B, Gandossi E, et al. The predictive value of ultrasound findings in the management of thyroid nodules. Q J Med. 2007;100(1):29–35.
4. Maroulis DE, Savelonas MA, Iakovidis DK. Computer-Aided Thyroid Nodule Detection in Ultrasound Images. In: Proc. of IEEE Symposium on Computer-Based Medical Systems (CBMS). Washington, DC, USA; 2005. p. 271–276.
5. Tsantis S, Dimitropoulos N, Cavouras D, Nikiforidis G. A hybrid multi-scale model for thyroid nodule boundary detection on ultrasound images. Comput Methods Programs Biomed. 2006;84(2-3):86–98.
6. Couprie C, Grady L, Najman L, Talbot H. Power Watersheds: A Unifying Graph-Based Optimization Framework. IEEE Trans Pattern Anal Mach Intell to appear;.
7. Allène C, Audibert JY, Couprie M, Cousty J, Keriven R. Some links between min-cuts, optimal spanning forests and watersheds; 2007.

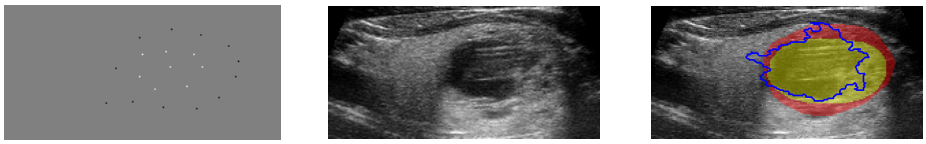

(a) Example 1: echo complex nodule, partly solid, partly cystic

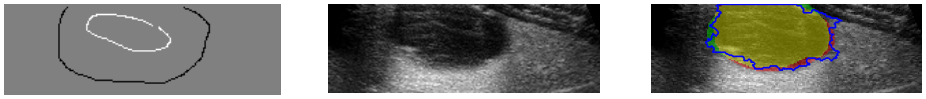

(b) Example 2: hypoechoic nodule, cystic

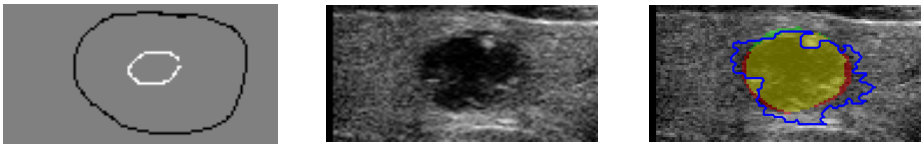

(c) Example 3: cyst

(d) Example 4: echo complex nodule

(e) Example 5: echo complex nodule

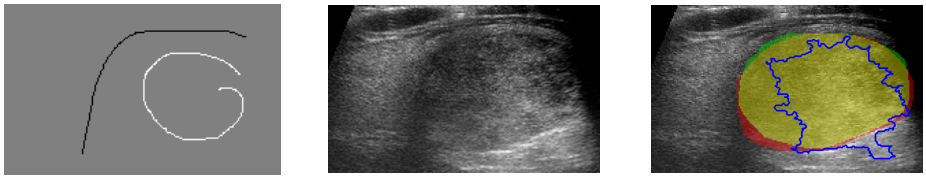

(f) Example 6 i): echo complex nodule

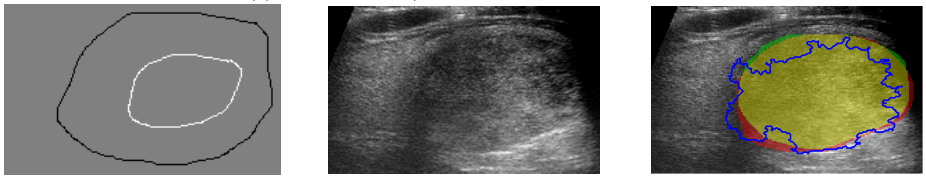

(g) Example 6 ii): echo complex nodule

Fig. 3. First column: segmentation mask (gray: area to segment, white: foreground, black: background); second column: original US slice; third column: manual gold standard segmentations (red, green; overlap: yellow) and PW segmentation result (blue). The sagittal section planes are shown. The diagnoses are listed below the subfigures. Example 6 i) and ii) show the result for two different input masks.